Direct Evidence of Fuel–Ablator Mix from Monochromatic Time-Gated Radiography in OMEGA Cryogenic Implosions

T. J. B. Collins, C. Stoeckl, R. Epstein, W. A. Bittle, C. J. Forrest, V. Yu. Glebov, V. N. Goncharov, D. R. Harding, S. X. Hu, D. W. Jacobs-Perkins, T. Z. Kosc, J. A. Marozas, C. Mileham, F. J. Marshall, S. F. B. Morse, P. B. Radha, S. P. Regan, B. Rice, T. C. Sangster, M. J. Shoup III, W. T. Shmayda, C. Sorce, W. Theobald, and M. D. Wittman

Laboratory for Laser Energetics, University of Rochester

In direct-drive inertial confinement fusion,[1] a shell is imploded via direct laser-light illumination. The shell is composed of an inner layer of fuel (typically equimolar deuterium and tritium, which maximizes yield) and a thinner outer "ablator" layer of non-fuel material (e.g., a CH polymer). The implosion of a two-layer shell filled with gaseous fuel is used to briefly assemble a "hot spot" of sufficiently high temperature (4 or more keV) and density for D–T fusion reactions to occur. The fusion neutron yield depends on the hot-spot conditions and the confinement time, the latter depending on the areal density of the shell and ablator at stagnation. Various phenomena can reduce the shell areal density, such as heating of the shell by suprathermal electrons generated in the corona surrounding the imploding target; shock dynamics, which must be carefully engineered due to the increase in entropy generated by mistimed shocks; absorption of coronal radiation by the shell, which places an additional constraint on the choice of ablator material; and mixing of the ablator and shell fuel material due to hydrodynamic instabilities, particularly the Rayleigh–Taylor instability (RTI).

In this summary we infer the degree of fuel–shell mixing using 2-D radiation-hydrodynamic modeling of two OMEGA cryogenic implosions. The properties of the two implosions in question are shown in Table I (with 1-D simulated data calculated using the radiation hydrocode *LILAC*[2]). Direct evidence that this is due to Rayleigh–Taylor fuel–ablator mixing in these two implosions was previously obtained using a Si He_α backlighter driven by an ~20-ps short pulse generated by OMEGA EP.[3] The shadow cast by the shell shortly before stagnation, as diagnosed using backlit radiographs, shows a softening near the limb, which is evidence of an ablator–fuel mix region for a low-adiabat implosion ($\alpha \sim 1.9$, in-flight aspect ratio IFAR = 14) but not for a moderate adiabat implosion ($\alpha \sim 2.5$, IFAR = 10). We consider various possible causes of fuel–shell mix, using the radiation-hydrodynamic code *DRACO*, and find good agreement between experimental and simulated radiographs when imprint is modeled and for a particular ablator thickness that lies within the range of possible thicknesses as determined by pre-shot target metrology. Modeling with *DRACO*[4] includes multigroup radiative transport, nonlocal electron heat transport, scattering due to cross-beam energy transfer,[5] and first-principles[6] equation of state and opacity models, and is post-processed with *Spect3D*[7] to generate synthetic x-ray images for direct comparison

Table I: Simulated and experimental properties of the moderate- and low-adiabat shots 81590 and 82717, respectively. The ratio of the pressure to the Fermi pressure at zero temperature is given by α; IFAR is the in-flight aspect ratio, the ratio of the initial shell radius to the thickness at a convergence of 1.5; T_i is the neutron-weighted ion temperature; ρR is the neutron-weighted areal density of the shell; ρR/clean is the ratio of measured to 1-D simulated areal density; and YOC is the ratio of experimental to 1-D yield.

LILAC (1-D)							Experiment		
Shot	α	IFAR	v_{imp} (km/s)	ρR (mg/cm^2)	$T_{i,LILAC}$ (keV)	Y_{LILAC} (10^{13})	ρR/clean	$T_{i,exp}$ (keV)	YOC
81590	2.5	10	240	250	2.2	1.4	78%	2.7	19%
82717	1.9	14	280	246	2.4	2.6	41%	2.4	8%

with experimental framing-camera images. Furthermore, because lineouts from synthetic radiographs of 1-D and 2-D simulations show good agreement for the moderate adiabat shot 81590 (see Fig. 1), we focus below on the lower-adiabat shot 82717. In the possible sources of mix described below, we begin with those found to be the less significant, concluding with the most significant, imprint.

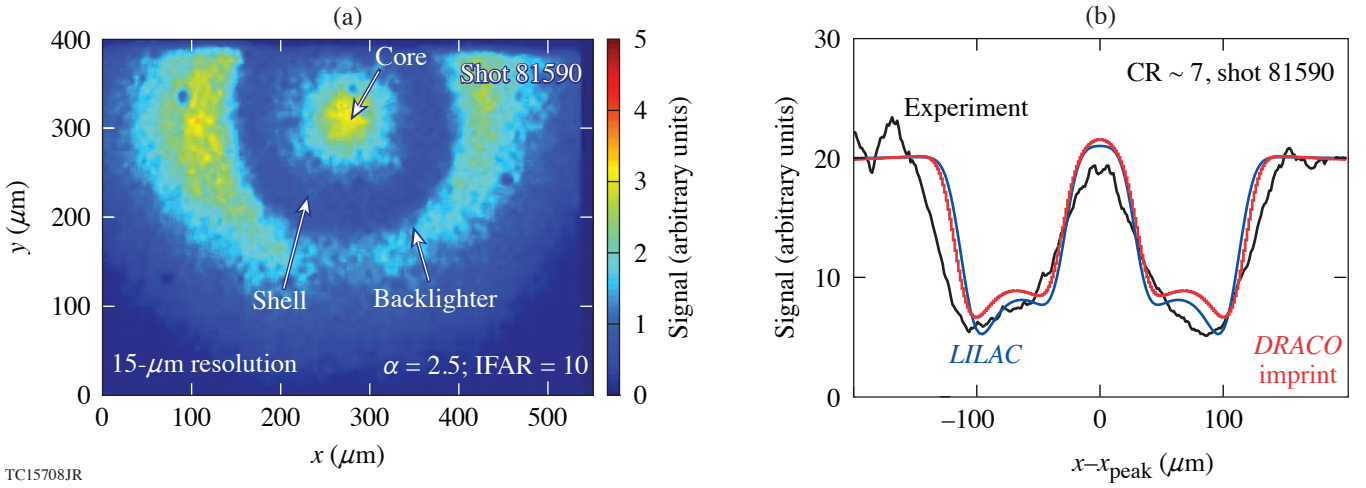

Figure 1
The (a) experimental radiograph for shot 81590 and (b) radiographic lineouts for the experiment (black curve), *LILAC* (blue curve), and *DRACO* (red curve), plotted as functions of the horizontal coordinate measured relative to the position of the peak core emission (x_{peak}). CR: convergence ratio.

Long-Wavelength Modes

The imploding shell is unstable to Rayleigh–Taylor and Richtmyer–Meshkov instabilities, which can be seeded by target and laser nonuniformities and imperfections. We modeled the effects of long-wavelength laser drive nonuniformities, including beam-to-beam power imbalance, and beam pointing error. Long-wavelength mode growth can also be seeded by nonuniformity in the inner edge of the DT ice, the greatest amplitudes of which occur for Legendre modes with modal index less than 10. The impact of these was found to be negligible in the fuel–ablator mix used for both shots, although perturbations with Legendre-mode indices 1 and 2 have a visible effect on the shape of the core emission and may be responsible for the slight elongation of the hot spot [Fig. 2(a)].

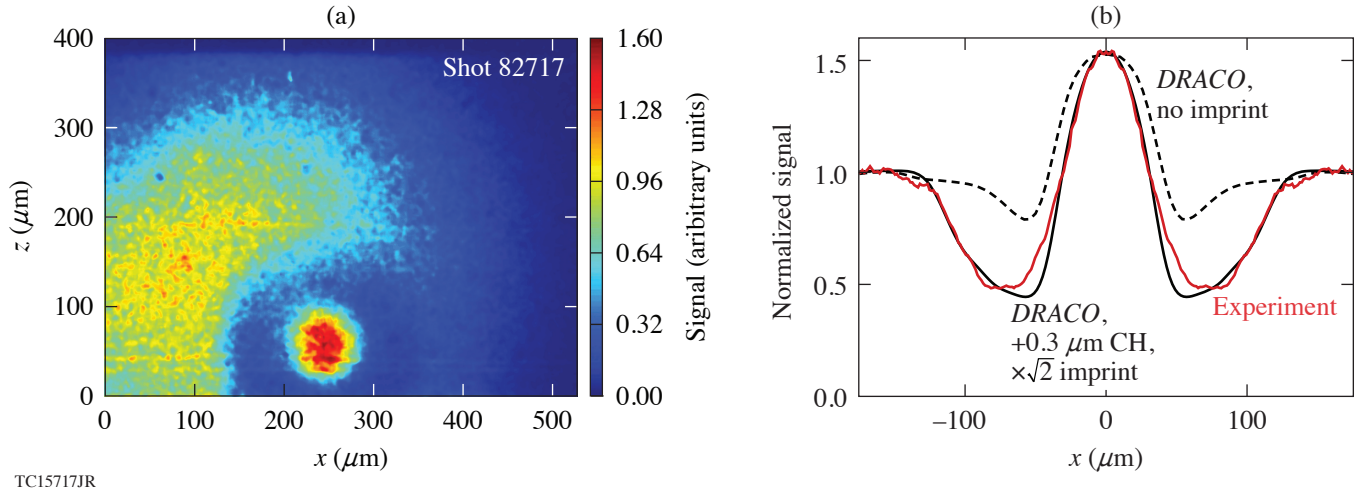

Figure 2
(a) The experimental radiograph for shot 82717 shows a hot central core (red) surrounded by a dark ring of shell absorption, further surrounded by the off-center backlighter emission. (b) Radiographic lineouts of shot 82717 for the experiment (red curve), symmetrized about $x = 0$, where x is the horizontal position in the image plane; a simulation without imprint (dashed black curve); and a *DRACO* simulation with imprint and an additional 0.3 μm of initial ablator thickness.

Kinetic Effects and Concentration Diffusion

Another mechanism investigated as a means of transporting carbon deep into the imploding shell is concentration diffusion. One of many kinetic effects that have received attention in recent years,[8] concentration diffusion is expected to occur wherever a concentration gradient exists in a multispecies plasma.[9] The flux in this case is given by Fick's law and is proportional to the concentration gradient. A second-order accurate ion concentration diffusion model was implemented in *DRACO* to investigate this effect. At the fuel–shell interface the concentration gradient scale length is small, being comparable to the mean-free path for the cold shell material. Due to the low temperatures and high densities, the concentration flux remains small throughout the implosion, increasing only upon complete ablation of the CH ablator, which occurs late in time. Once the CH is ablated, the temperature quickly rises and the density drops, causing the diffusion coefficient to rise; however, the region where the concentration gradient is large has also ablated. Therefore, concentration diffusion is able to flux material within the corona but not within the shell.

Classical Instability Growth at the Fuel–Ablator Interface

One natural source of mix to consider is perturbation growth at the fuel–ablator interface seeded by perturbations on that surface. Unlike at the ablation surface, growth of modes here due to the RTI is not diminished by ablation, so no high-mode ablative cutoff exists. Beta decay from tritium decay in permeation-filled–target cases causes localized damage at the inner shell surface, potentially seeding the perturbation growth. This may play a role in the known relationship between target age and performance.[10] In addition, the surface roughness of the polystyrene ablator shell may seed perturbation growth. A simulation of shot 82717 was performed with a piecewise power-law function approximating the measured polystyrene power spectrum and was repeated with the spectrum multiplied by various multiples. For the nominal case, the effects of the perturbation are small and have a negligible impact on the shell mass density. For the enhanced simulation, the impact is more significant on the shell mass density, but there is still minimal material mixing due to perturbation growth.

Laser Imprint

For the lower-adiabat shot, 82717, the radiograph lineout from a 1-D simulation fails to match either the radial extent (width) or depth of the shadow cast by the shell. *DRACO* simulations were performed with the expected level of laser imprint, as well as for enhanced levels in which the imprint spectrum was multiplied by factors of $\sqrt{2}$ and 2. These simulations were able to reproduce the depth of the shell shadow but not the width, the closest agreement in the shell depth being found for the $\sqrt{2}$ simulation. Because 3-D perturbations are known to grow more quickly than 2-D perturbations, the need for an enhanced imprint spectrum in a 2-D simulation is expected.[11]

The discrepancy in the depth of the shell shadow has a ready explanation in the markedly greater bound–free absorption of the CH compared to the free–free absorption of the DT fuel. A survey of simulations with the same shell mass but different initial ablator thickness shows that an ablator thickness of 0.3 μm has a marked impact on the thickness of the shell shadow. A radiographic lineout from a simulation using an ablator thickness of 11.5 μm and incorporating enhanced imprint shows a close agreement with the experimental data (Fig. 2). It should be noted that the impact of ablator thickness on the shadow width and imprint on the shadow depth are independent; increasing the degree of imprint fails to increase the thickness of the shadow, and increasing the ablator thickness alone cannot reproduce the depth of the shadow without making it far too wide. The important result of this study is that the experimental radiograph is only reproduced by enhanced imprint (not unexpected) combined with an ablator that lies within the measured range of 10.9 μm to 11.5 μm but lies at the upper limit of the range of uncertainty of the measurement. The latter observation allows two possible inferences: (a) The actual ablator thickness was within the measurement error, or (b) the ablator thickness was actually smaller but the simulated ablation rate exceeded the experimental rate, a possibility suggested by previous warm-target implosions.[12] This suggests value in developing and investing in higher-precision target metrology.

In conclusion, two OMEGA cryogenic implosions were backlit by OMEGA EP, obtaining radiographs of the hot-spot and stagnation fuel–shell assembly close to peak convergence. The implosions were designed to lie on either side of the stability threshold, and both simulations and experimental data bear this out. Modeling of the moderate-adiabat implosion agrees well with experiment, as expected. Modeling of the low-adiabat implosion agrees when an enhanced level of imprint is modeled, and only when a sufficiently thick ablator (within measurement error) is assumed.

This material is based upon work supported by the Department of Energy National Nuclear Security Administration under Award Number DE-NA0003856, the University of Rochester, and the New York State Energy Research and Development Authority.

1. R. S. Craxton *et al.*, Phys. Plasmas **22**, 110501 (2015).
2. J. Delettrez *et al.*, Phys. Rev. A **36**, 3926 (1987).
3. R. Epstein *et al.*, High Energy Density Phys. **23**, 167 (2017); C. Stoeckl *et al.*, Phys. Plasmas **24**, 056304 (2017).
4. P. B. Radha *et al.*, Phys. Plasmas **23**, 056305 (2016); I. V. Igumenshchev *et al.*, Phys. Plasmas **17**, 122708 (2010).
5. C. J. Randall, J. J. Thomson, and K. G. Estabrook, Phys. Rev. Lett. **43**, 924 (1979).
6. J. J. MacFarlane *et al.*, High Energy Density Phys. **3**, 181 (2007).
7. S. X. Hu *et al.*, Phys. Rev. B **84**, 224109 (2011); S. X. Hu *et al.*, Phys. Rev. E **92**, 043104 (2015); S. X. Hu *et al.*, Phys. Rev. E **90**, 033111 (2014); S. X. Hu *et al.*, Phys. Plasmas **25**, 056306 (2018).
8. P. Amendt *et al.*, Phys. Plasmas **18**, 056308 (2011).
9. R. B. Bird, W. E. Stewart, and E. N. Lightfoot, *Transport Phenomena*, Revised 2nd ed. (John Wiley & Sons, Inc., New York, 2007).
10. E. M. Campbell *et al.*, Phil. Trans. R. Soc. A **379**, 20200011 (2020); A. Lees *et al.*, Phys. Rev. Lett. **127**, 105001 (2021).
11. M. M. Marinak *et al.*, Phys. Rev. Lett. **80**, 4426 (1998); R. Yan *et al.*, Phys. Plasmas **23**, 022701 (2016).
12. D. T. Michel *et al.*, High Power Laser Sci. Eng. **3**, e19 (2015).